Journal of Materials Chemistry A

Accepted Manuscript

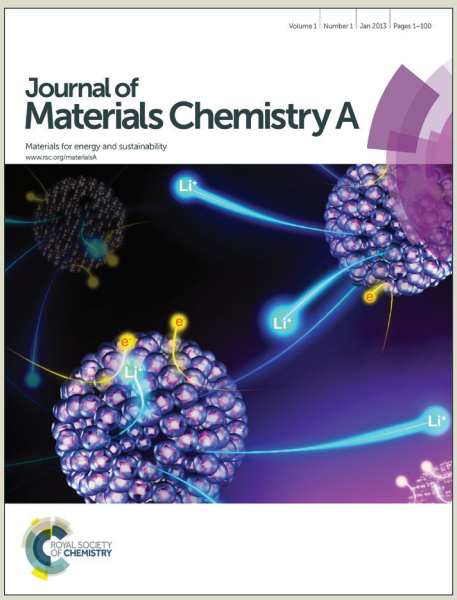

ROYAL SOCIETY OF CHEMISTRY

www.rsc.org/materialsA

Nitrogen-doped Graphene-Supported Cobalt Carbonitride@Oxide Core-Shell Nanoparticles as a Non-noble Metal Electrocatalyst for Oxygen Reduction Reaction

Yingsi Wu, Qianqian Shi, Yuhang Li, Zhuangchai Lai, Hao Yu*, Hongjuan Wang, Feng Peng*

A new catalyst, cobalt carbonitride (CoCN) nanoparticles supported on nitrogen-doped graphenes (NG), was synthesized via a high temperature ammonia nitridation method. The catalyst has a core-shell structure with a highly active CoCN core and a protective cobalt oxide shell. Linear sweep voltammetry measurements show that the catalyst presents excellent activity in oxygen reduction reaction compared to cobalt oxide supported on NG and commercial Pt/C catalysts, benefiting from the strong synergistic effect between CoCN and NG and the electronic modification of cobalt oxide by CoCN from within.

Introduction

Improving the oxygen reduction reaction (ORR) performance on cathodes is essential for commercializing polymer electrolyte membrane fuel cells (PEMFCs), because its sluggish kinetics is responsible for two thirds of the overpotential in a fuel cell based on state-of-the-art platinum catalysts.[1] Consequently, ~90% Pt catalysts are needed on cathodes.[2] It is crucial to develop new catalytic materials to replace the Pt-based cathodic catalysts due to the high cost, limited supply and unstable activity of Pt.

Non-noble metal catalysts, such as transition metal oxides,[3] chalcogenides,[4] carbides[5] and transition metal macrocyclic complexes[6] are promising alternatives for their low costs and good catalytic performance. Early transition metal nitrides (TMNs) and carbides (TMCs) are regarded as promising substitutes for noble metal catalysts, because of their Pt-like electronic behaviors, derived from the changes in lattice parameter and electron density due to the addition of N or C atoms.[7, 8] So far, the nitrides, carbides, oxynitrides and carbonitrides of group IV-VI metals, including TiN, MoC, Mo_2N, HfO_xN_y and TaCNO etc.,[9-13] have been documented for ORR, among which the structure and properties of Mo nitrides are the most studied. Mo nitride supported on carbon (Mo_2N/C) was used for ORR in acid solution and showed a good stability, with an electron transfer number of four.[11] Although these catalysts show improved stability in ORR, their activities are still low compared with commercial Pt/C catalysts. The nitrides of higher group VII-VIII metals showed excellent activity in hydrodenitrogenation and hydrodesulfurization reactions.[14, 15] However, they are less stable in oxidative reactions, because the thermodynamic stability of TMNs decreases with the increase of the atomic radius as larger atoms cannot accommodate the interstitial nitrogen.[16] Engineering the composition of group VII-VIII by forming bi-metallic nitrides[17] or creating oxynitrides[18] may enhance the stability, meanwhile the activity may be improved by surface oxygen vacancies as well. Our previous work demonstrated that CoN supported on Al_2O_3 is a good catalyst for the preferential CO oxidation.[19] Cao et al. reported that bimetallic Co-Mo oxynitrides exhibit moderate ORR activity in acidic conditions and superb activity in alkaline conditions

approaching that of Pt/C catalysts.[20]

In 2009, the pioneering work from Dai and co-workers opened the possibility to develop metal-free ORR catalysts based on carbons and their nitrogen-doped derivatives.[21] Since then, heteroatom doped graphenes received particularly attentions because of their activity and stability as ORR electrocatalysts, owing to their unique 2-D structure and electronic properties.[22-25] Furthermore, the synergistic effect of transition metal-carbon system may offer exceptional enhancement for ORR performance. For example, Co_3O_4 supported on N-doped graphene showed significantly improved activity in alkaline solution compared to Co_3O_4 and N-doped graphenes alone.[26] Iron strongly interacted with graphenes plays a central role for the excellent activity of double-walled-CNT-derivated graphenes in both acid and alkaline conditions.[27] Very recently, a superior performance to Pt/C were achieved in alkaline solution by maximizing the interaction between FeN and 3-D N-doped graphenes using FePc as precursor.[28]

Herein, we report the fabrication of N-doped graphene supported cobalt carbonitride (CoCN) and its excellent performance approaching Pt/C in ORR in alkaline solution. The catalyst was prepared by nitridation of graphite oxide supported cobalt hydroxide in NH_3. Highly dispersed CoCN nanoparticles (NPs) were stabilized by passivation with a 2 nm thin cobalt oxide (CoO_x) shell. It was demonstrated that the encapsulated CoCN cores alter the oxygen activation and reduction on oxide shells. The synergistic effect of N-doped graphene and CoCN@CoO_x core-shell structure enabled an excellent performance in ORR under alkaline conditions,

approaching that of commercial Pt/C with similar metal loading.

Experimental

Preparation of graphene oxide

Graphene oxide (GO) was synthesized with a modified Hummers method.[29] Firstly, 3 g graphite was added into a mixture of concentrated H_2SO_4 (30 mL), $K_2S_2O_8$ (2.5 g), and P_2O_5 (2.5 g) and the solution was maintained at 80 °C for 4.5 h. The resulting pre-oxidized graphite was diluted with deionized (DI) water, filtrated, dried and then added to 120 mL of concentrated H_2SO_4. 15 g of $KMnO_4$ was added slowly to the ice-cooled mixture (<20 °C) and the mixture was stirred at 35 °C for 2 h, diluted with 250 mL of DI water and stirred for additional 2 h. After adding 700 mL of DI water, 30% H_2O_2 solution (20 mL) was added dropwise. The color of the solution turned to bright yellow. The product was collected by standing and filtration and was washed by 8 L H_2O/HCl (9/1, v/v) solution. Then the mixture was re-dispersed in DI water to 8 g/L and dialyzed for 1 week until the dialysate was neutral to obtain GO. The GO was exfoliated in DI water by sonication for 2 h. The concentration of the suspension was 1 mg/mL.

Synthesis of CoCN@CoO_x/NG

An appropriate amount of cobalt acetate ($Co(OAc)_2$) aqueous solution was added into 200 mL of GO solution dropwise under stirring. The mixture was then stirred overnight, followed by adding 0.2 mL $NH_3 \cdot H_2O$. The suspension was refluxed at

80 °C for 4 h to obtain the precursor $Co(OH)_2$/GO. Then, N-doped graphene (NG) supported CoCN was prepared by a temperature-programmed reaction and pyrolysis of the precursor in 30% NH_3/Ar gas mixture at 700 °C for 2 h.[19] The sample was cooled to room temperature in the same atmosphere then purged with Ar for 10 min, then was passivated in 1% O_2/Ar for 2 h before exposed to air, which resulted in the formation of CoCN@CoO_x(*y*)/NG, where *y* in brackets represents the loading of Co. To completely oxidize the CoCN NPs to cobalt oxide, CoCN@CoO_x(18)/NG was heated in air at 350 °C for 2 h. The resulted material is denoted as h-Co_3O_4/NG, where *h* stands for hollow NPs. 3 M HCl was used to wash cobalt species on CoCN@CoO_x(5)/NG with 30 min sonication. The resulted sample is denoted as washed-NG. The nomenclature, mass fraction of cobalt, nitrogen and oxygen contents and specific surface area of all the catalysts used in this work were summarized in Table S1.

Synthesis of bulk samples

Bulk $Co(OH)_2$ precursor was prepared as the method above without adding GO. CoO was prepared by heating $Co(OH)_2$ in Ar atmosphere at 500 °C for 2 h. Bulk cobalt nitride was obtained by the nitridation of $Co(OH)_2$ with 30% NH_3/Ar gas mixture at 700 °C for 2 h and then passivation at room temperature with 1% O_2/Ar. The passivation step was employed to form thin oxide layers to avoid serious oxidation of nitride as exposed to air.[19, 30] The sample is denoted as CoN for simplicity. Further oxidizing the CoN at 350 °C for 2 h in air resulted in Co_3O_4 sample (see Fig. S1).

To evaluate the synergistic effect between CoCN and GO, we mixed CoO and GO by grinding, then nitridated the mixture with 30% NH_3/Ar, during which CoN may be carbonized by GO to form CoCN. The sample is denoted as CoCN/NG. As a comparison, CoN and washed-NG were directly mixed by grinding, which is referred to CoN+washed-NG. The contents of CoCN/CoN in CoCN/NG and CoN+washed-NG samples were about 70 wt%.

Characterizations

Transmission electron microscopy (TEM) measurements were conducted on a FEI Tecnai G2 12 operated at 100 kV and a JEM-2100F connected with an electronic energy loss spectroscopy (EELS) detector performed at 200 kV. X-ray diffraction (XRD) patterns were collected by a D8-advance X-ray diffractometer (Bruker, Germany) with Cu Ka radiation (40 kV, 40 mA) at a scan rate of 1°/min. For samples with lower degree of crystallinity, a slower scan rate of 0.5°/min was applied. Raman spectra were recorded on a LabRAM Aramis micro Raman spectrometer with 633 nm wavelength laser and 2 μm spot size. X-ray photoelectron spectroscopy (XPS) data were obtained by a Kratos Axis ultra DLD equiped with Al Ka X-ray source. All XPS spectra were calibrated by setting the graphitic C 1s signal to 284.6 eV and were fitted after a Shirley type background subtraction. Measurements of specific surface area and pore volume were operated in a Micromeritics ASAP 2010 apparatus. Elemental analysis results were taken using Vario EL III (Elementar, Germany). The contents of element Co were measured using atomic adsorption spectroscopy (Hitachi Z-5000).

Electrochemical tests

Typically, 1 mg of catalyst was dispersed in 0.5 mL solvent mixture of Nafion (5%), DI water and acetone (V : V : V = 15 : 385 : 100) by sonication to form a catalyst ink. 10 μL catalyst ink was dropped onto the pre-polished glassy carbon (GC) surface and was dried at room temperature. The diameter of electrode was 5.0 mm for linear sweep voltammetry (LSV) measurements and the catalyst loading was approximately 0.102 mg cm^{-2}.

Electrochemical measurements were carried out in an electrochemical analyzer (Eco Chemie B. V. Autolab PGSTAT30) and a rotator (Pine Instrument Co) with a three-electrode cell system. GC casted with catalysts, Ag/AgCl with saturated KCl and Pt wire were used as the working electrode, reference electrode and counter electrode, respectively. For comparison, commercial Pt/C (20 wt% Pt, Johnson-Matthey) working electrode was prepared as the procedure described above. LSV measurements were conducted at rotation speeds varying from 400 to 2800 rpm with the scan rate of 10 mV/s. The electrochemical impedance spectroscopy (EIS) was performed in the 0.1 M KOH solution at a constant potential of −0.1 V in the frequency range from 0.1 to 100,000 Hz.

Calculation methods

Density functional theory (DFT) calculations were performed with the DMol3 package[31] in Materials Studio 6.1. Exchange-correlation functions were described by generalized gradient approximation (GGA) with Perdew-Burke-Emzerhof (PBE).[32]

DFT Semi-core Pseudopots (DSPPs) was adopted for the core treatment. Double numerical plus polarization (DNP) was employed as the basis set and the orbital cutoff of 4.5 Å was assigned to global atoms. The convergence tolerance of self-consistent field (SCF) calculations was 1.0×10^{-6} Ha. For the geometry optimization, the convergence in energy and the maximal force were 1.0×10^{-5} Ha and 2.0×10^{-3} Ha/Å, respectively. The smearing value of 0.002 Ha was used to relax the structures, while there was nonuse of smearing for energy calculations. The k-point of the first Brillouin zone was set to 12×12×1.

Co_4N, in which a nitrogen atom is located at the center of cubic-lattice cell of cobalt, was used to model the cobalt nitride. After the geometry optimization, lattice parameters of a, b and c are all 3.61 Å. We cleaved the (1 1 1) surface of Co_4N, then covered it with CoO to mimic the core@shell structure. Two layers of (1 1 1) surface of CoO was constructed on the top of Co_4N (1 1 1) surface with four atomic layers. In order to match the cell of Co_4N, lattice parameters of CoO were set to be equal to Co_4N. To avoid the interaction between adjacent cells, a vacuum layer of 15 Å was added above the surface. All atoms of catalyst were fixed when calculated the adsorption properties of oxygen.

Results and discussion

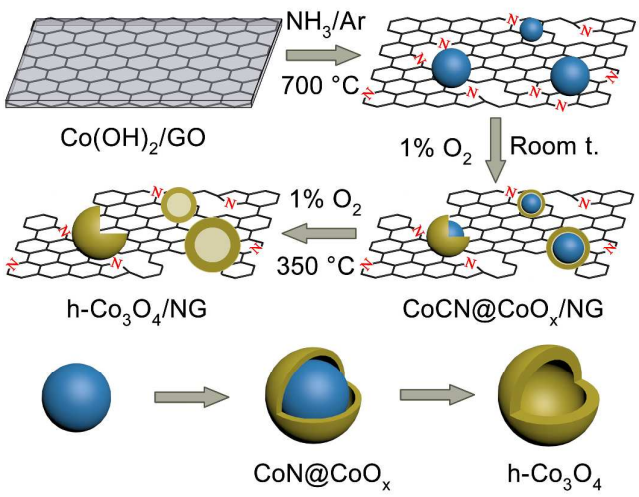

Scheme 1 Schematic diagram of synthesizing CoCN@CoO_x/NG and cobalt oxide NPs on NG.

Scheme 1 illustrates the two-step procedure for synthesizing the catalysts used in this work. The synthesis was started from GO supported cobalt hydroxide, denoted as $Co(OH)_2$/GO, which was prepared by the hydrolysis of $Co(OAc)_2$ assisted by aqueous ammonia.[33] It was then subjected to a high-temperature nitridation in NH_3 at 700 ^oC to convert $Co(OH)_2$ to the corresponding nitride and to introduce N-dopant into graphenes. The resulted cobalt nitride was extremely active, which catalyzed the oxidation of graphene support, resulting in rapid ignition of the solids as exposed to air. A room-temperature oxidation with 1% O_2[19, 30] was used to prevent the nitride from excessive oxidation by forming an oxide layer on the surface of nitride NPs, maintaining the core as cobalt nitride. It should be mentioned that, even under the mild condition, the high activity of CoN may result in strong interaction between NPs and their surrounding environments, as discussed in following section. For comparison, the passivated sample can be further oxidized to convert the nitride core to oxide at 350 ^oC. Because of the outward diffusion of nitrogen (similar to the Kirkendall effect), the oxidation of nitride core generated hollow Co_3O_4 spheres

supported on NG, which was used to investigate the role of surface oxide layer in ORR.

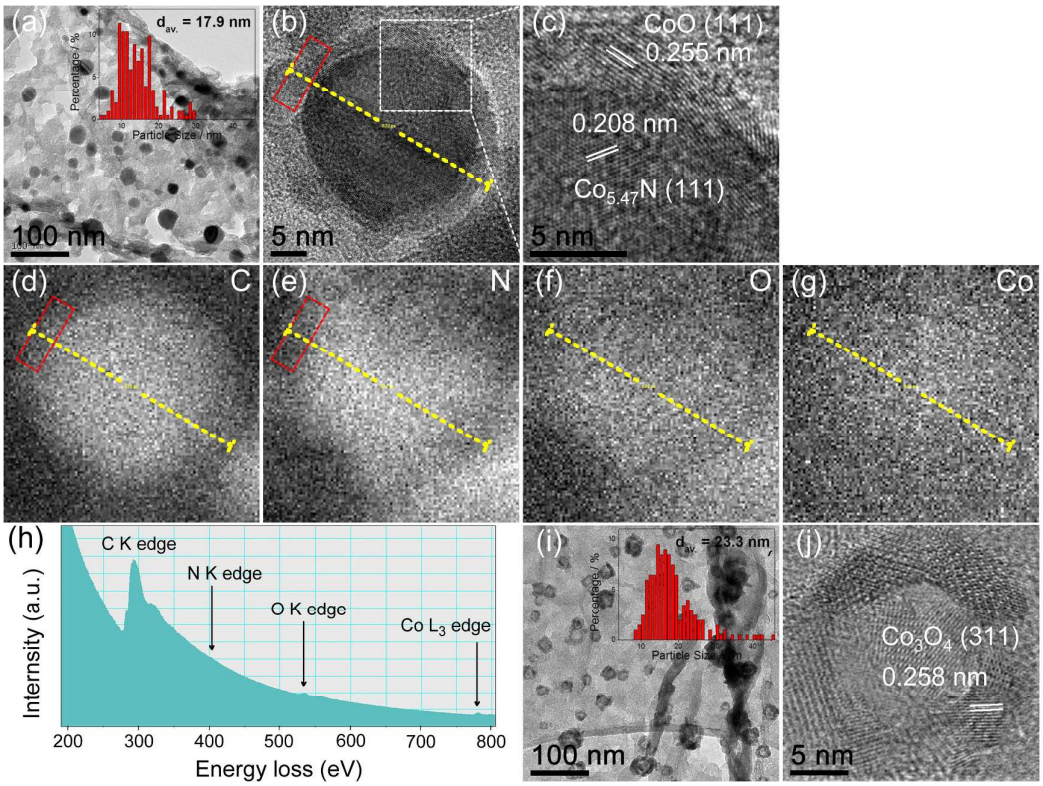

Fig. 1 (a-c) Low and high resolution TEM images of CoCN@CoO_x(18)/NG. (d-g) Elemental mappings of carbon, nitrogen, oxygen and cobalt by high resolution EELS. (h) Typical EELS spectrum of CoCN@CoO_x(18)/NG . (i, j) Low and high resolution TEM images of h-Co_3O_4/NG.

Figs. 1a-c show TEM images of the CoCN@CoO_x(18)/NG sample. The sizes of NPs on NG were in the range from 5 to 30 nm and centered at 17.9 nm. A close HRTEM observation clearly revealed the core@shell structure of the NPs. As shown in Fig. 1b, a 2-3 nm thin shell with low contrast covers the core NP of about 13 nm in diameter. The distance between fringes of the shell corresponds the (111) planes of CoO, and the fringes in core area can be attributed to the (111) planes of $Co_{5.47}N$ intermetallic compound, suggesting that the core@shell particles are composed of cobalt nitride encapsulated by cobalt oxide. We used HREELS mapping to determine

the elemental distribution across the particle. As shown in Figs. 1d-h, nitrogen obviously enriched in the central core area while was lacking in the shell represented by the red rectangular. It should be noted that the particle, especially in the core, contains considerable carbon atoms, as shown in Fig. 1d, manifesting that the composition of the particle is actually carbonitride or there exists a carbide layer surrounding the core. The formation of carbonitride indicates the interaction between graphene and cobalt domains. At high temperatures, $Co(OH)_2$ may be reduced by NH_3[34] or graphenes[35] to form metallic particles, which can accommodate either carbon or nitrogen atoms to form intermetallic carbonitride compound.

It was noticed that obvious mesopores were created on graphenes, turning 2-D graphenes into a mesoporous support, as shown in Fig. 1a. More TEM observations showed that the pores usually appeared near the CoCN@CoO_x particles in the form of worm-like tortuous trenches on graphene sheets (see Fig. S2). It can be explained by the etching of carbon by oxygen catalyzed by nitride particles, being similar to the catalytic gasification of graphite in the presence of transition metals or their compounds, e.g. Ag and CeO_2.[36, 37]

Fig. 1i displays the TEM image of h-Co_3O_4/NG obtained through the complete oxidation of CoCN@CoO_x(18)/NG. The diffusion of nitrogen from inner cores toward outer surfaces led to the formation of hollow structure.[38] A statistic of TEM images indicated that the hollow Co_3O_4 particles have an average outer diameter of 23.3 nm and wall thickness of about 4 nm. Supposing a CoCN core in 17.9 nm average diameter has been completely transformed into the Co_3O_4 shell, the outer

diameter of the hollow NP will be 22.4 nm, being close to the observed value 23.3 nm. The HRTEM image in Fig. 1j shows clear lattice fringes from Co_3O_4 crystallites.

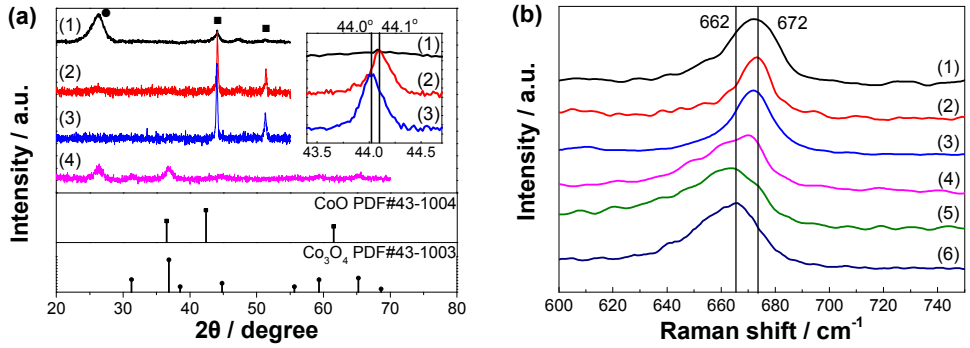

Fig. 2 (a) XRD patterns of (1) CoCN@CoO_x(18)/NG, (2) CoCN@CoO_x(63)/NG, (3) CoN and (4) h-Co_3O_4/NG. (●) Graphite, (■) CoN. (b) Raman spectra of (1) CoCN@CoO_x(18)/NG, (2) CoCN@CoO_x(63)/NG, (3) CoN, (4) h-Co_3O_4/NG, (5) CoO and (6) Co_3O_4.

The formation of carbonitride was also supported by XRD and Raman analysis. Fig. 2a presents the XRD patterns of the synthesized catalysts. For the CoCN-containing samples (1, 2), the diffraction peaks at 44° and 51°correspond to (111) and (200) reflections of cobalt nitride intermetallic compound ($Co_{5.47}N$, JCPDS 41–0943). The accommodation of carbon in the lattice can be proved by comparing the (111) reflection of CoCN with that from CoN prepared in the absence of graphenes. An obvious shift of CoCN (111) towards higher angle side can be observed. Since the interaction between carbon and supported metals is generally too weak to result in strains in catalyst crystallites,[39-41] it is indicative of the existence of carbon with smaller atomic radius, which causes the lattice contraction.[42] The XRD analysis also demonstrated that the hollow particles in sample h-Co_3O_4/NG were composed of phase-pure Co_3O_4. Figs. 2b and S3 (see ESI) show the Raman spectra of the catalysts. In Fig. S3, the peaks around 190 and 515 cm^{-1} correspond to the $F_{2g(1)}$ and $F_{2g(2)}$

symmetry modes of Co_3O_4.[43] The bands around 467 and 662 cm^{-1} can be assigned to the $E_{g(1)}$ and A_{1g} symmetry modes of Co_3O_4[43] or CoO[44], because of the possible oxidation of CoO when exposed to excitation laser.[45] Fig. 2b shows the close observation of A_{1g} symmetry mode. Compared with CoO and Co_3O_4 samples, the CoCN-containing samples shift the A_{1g} band toward high frequency side by about 10 cm^{-1}, because the insertion of N/C atom modifies the vibration of Co-O bond. Similar results have been reported in the Raman analysis of TiO_2 and TiN materials.[46]

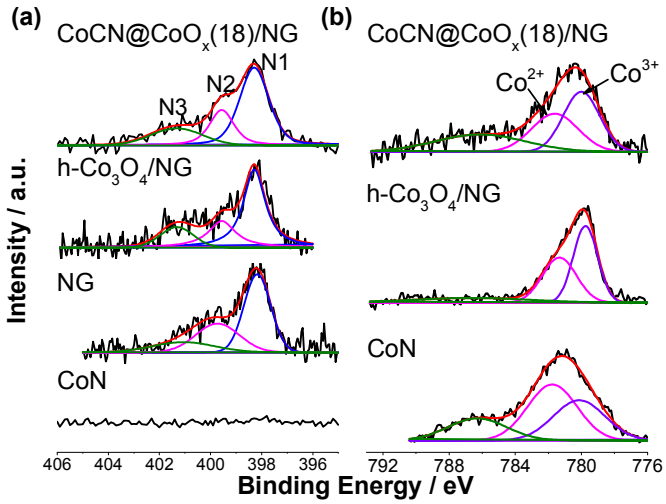

Fig. 3 XPS high resolution (a) N 1s and (b) Co 2p3/2 spectra of CoCN@CoO_x(18)/NG, h-Co_3O_4/NG, NG and CoN.

Afore results demonstrated that the CoCN@CoO_x(18)/NG catalyst has a core@shell structure with a CoCN core in a very thin oxide shell. Since the catalysis takes place on surfaces, more detailed information on the chemical status of shells is desired to help determine the nature of active sites. Figs. 3a and b show the N1s and Co2p3/2 regions of XPS spectra of CoCN@CoO_x(18)/NG, h-Co_3O_4/NG and NG samples. Both of NG as supports and CoCN NPs might contribute to the N1s peaks. However, the surface nitrogen contents of CoCN@CoO_x(18)/NG, h-Co_3O_4/NG and

NG are very close, displaying similar contents of pyridinic (N1, 398.3 eV), pyrrolic (N2, 399.6 eV) and quaternary (N3, 401.3 eV) nitrogen (see Table S2 for quantitative results). This result implies that the CoCN core@shell particles contribute negligible N content, and CoCN NPs are encapsulated in continuous oxide shells, but not oxynitride. This conclusion was supported further by the N1s spectrum of CoN sample prepared in absence of graphene. With the same nitridation and passivation steps, no any N1s peak can be detected by XPS on the CoN sample, indicating the shells do not contain nitrogen within the analytical depth of XPS technique. While elemental analysis of CoN gives a 3.2 wt% N content in the sample, suggesting N is concentrated in the center of the particles. Cao et al. have synthesized Co-Mo bi-metallic oxynitride with similar method.[20] In our work, the complete oxidation of surface nitride may be caused by the high activity of CoN. On one hand, it resulted in the relatively low resistance to oxidation compared to Co-Mo compounds; on the other hand, the high activity may be involved in the activation of oxygen in ORR, evidenced by the strong interaction with graphenes. Co 2p peaks of CoCN@CoO_x(18)/NG and CoN show the co-existence of Co^{2+}(780.6 eV) and Co^{3+}(779.6 eV) on catalyst surfaces. Although it is hard to distinguish Co-N and Co-O bonds by XPS,[47] we assigned the Co 2p peaks as cobalt oxides, because of the excluded effect of surface nitride as discussed above. On CoCN@CoO_x(18)/NG and CoN, the shake-up satellite peak at 786.3 eV is indicative of CoO,[48] suggesting that the oxide shell is composed of CoO and Co_3O_4. After oxidation at 350 ^oC, the satellite peak disappeared, indicating the hollow spherical particles in Figs. 1i-j are mainly

composed of Co_3O_4, agreeing with the XRD and Raman results. Compared with nanosized CoCN@CoO_x(18)/NG and h-Co_3O_4, the bulk CoN sample shows lower intensity ratio of Co^{3+}/Co^{2+}, implying the better performance may be achieved with the nanosized catalysts, because the amount of Co^{3+} on the surface of cobalt oxides has a positive influence on the ORR activity.[49]

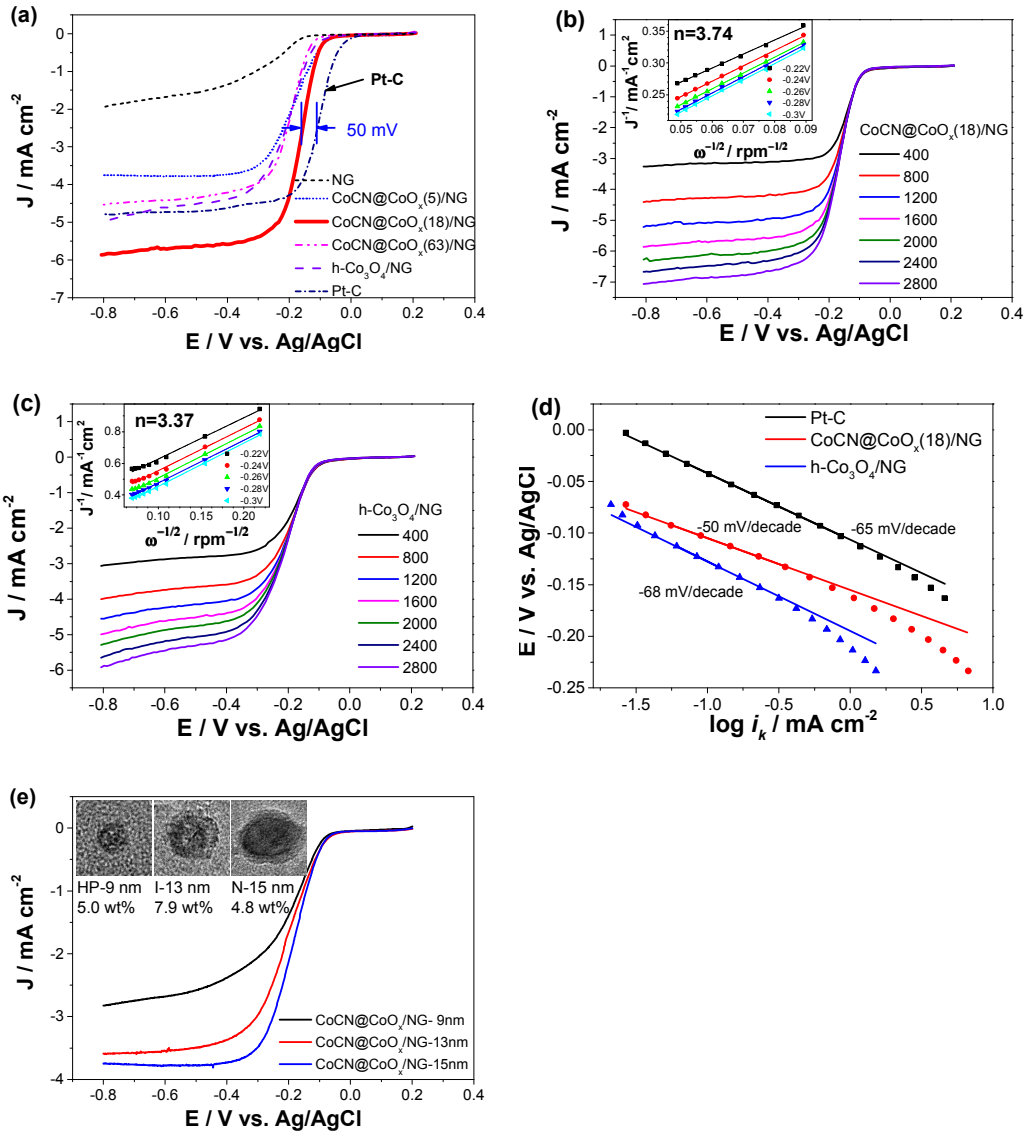

Fig. 4 (a) LSV curves of NG, CoCN@CoO_x(5)/NG, CoCN@CoO_x(18)/NG, CoCN@CoO_x(63)/NG, and Pt/C in O_2-saturated 0.1 M KOH solution at 1600 rpm rotating speed with a scan rate of 10 mV/s. (b, c) LSV curves of CoCN@CoO_x(18)/NG and h-Co_3O_4/NG at

various rotating speeds with a scan rate of 10 mV/s in O_2-saturated 0.1 M KOH solution; the insets are the calculated K–L plots at -0.22, -0.24, -0.26, -0.28 and -0.30 V vs. Ag/AgCl. (d) Tafel plots of CoCN@CoO_x(18)/NG, h-Co_3O_4/NG and Pt/C derived from RDE data at 1600 rpm in O_2 saturated 0.1 M KOH. (e) LSV curves of CoCN@CoO_x/NG with different particle sizes in O_2-saturated 0.1 M KOH solution at 1600 rpm rotating speed with a scan rate of 10 mV/s (see Figs. S5-S6, Table S4 in ESI).

Fig. 4a compared the LSV curves of CoCN@CoO_x/NG with different CoCN loadings and h-Co_3O_4/NG measured on rotating disk electrode (RDE) at 1600 rpm in O_2-saturated 0.1 M KOH solution. The bare NG material showed a slow current density increase with voltage sweeping. The introduction of CoCN significantly improved the activity, indicating the major contribution of CoCN@CoO_x to catalyst performance. By loading 5 wt% and 18 wt% Co, the diffusion limited current density at -0.8 V increased from 3.74 to 5.86 mA/cm^{-2}, meanwhile the onset potential remained the same. Increasing the Co element amount to 63 wt% resulted in decreased current density, probably due to the serious aggregation of catalyst on graphenes at the high loading amount. Compared with commercial Pt/C catalysts, CoCN@CoO_x(18)/NG displayed a current density of 5.62 mA cm^{-2} at -0.5 V, higher than that of Pt/C (4.70 mA cm^{-2}), and a half-wave potential of -0.16 V, being very close to that of Pt/C (-0.11 V). Taking into account the similar loading amount of active component (18 wt% Co vs. 20 wt% Pt) and the much lower cost of cobalt, the performance of CoCN@CoO_x(18)/NG is quite appealing. By comparing half-wave potentials and current densities at -0.5 V (see Table S3), CoCN@CoO_x(18)/NG can be regarded as a competitive Pt-free catalysts in alkaline conditions, offering comparative activity with C-COP-P-Co[50] and NT-G,[27] after Fe_xN/NGA.[28]

In this work, the CoCN NPs were coated by oxide layers, which protect CoCN

from oxidation but hinder the direct interaction between oxygen and CoCN. It is interesting to arise a question how the CoCN participates in the ORR without direct contact. It is widely documented that either CoO[51] or Co_3O_4[26] nanocrystallines are active ORR electrocatalysts. Therefore, comparing the performances of CoCN@CoO_x(18)/NG and h-Co_3O_4/NG deviated from the former may help evaluate how the CoCN core participates in the reaction. As shown in Figs. 4b and c, at 1600 rpm, the current density of h-Co_3O_4/NG was 4.52 mA cm^{-2} at -0.5 V and half-wave potential was -0.21 V, demonstrating the higher activity of core@shell particles than hollow Co_3O_4 shells. To investigate the kinetics, the Koutecky-Levich (K-L) plots (J^{-1} vs. $\omega^{-1/2}$) were obtained using LSV curves performed at various rotating speeds (see ESI for calculation). As shown in insets of Figs. 4b and c, the K-L plots of CoCN@CoO_x(18)/NG and h-Co_3O_4/NG exhibit good linearity at various potentials, suggesting that the reactions follow the first order kinetics. The electron transfer numbers, *n*, of CoCN@CoO_x(18)/NG, h-Co_3O_4/NG and Pt/C were 3.74, 3.37 and 4(Fig. S4), respectively, indicating the more efficient 4-electron reduction on CoCN@CoO_x(18)/NG. In addition, an elemental analysis and N_2-adsorption test showed that the complete oxidation of CoCN@CoO_x(18)/NG resulted in slight increases of the content of Co and specific surface area (see Table S1), due to the partial gasification of graphenes and the formation of hollow cavities of h-Co_3O_4. The XPS analysis shown in Fig. 3 exhibited their similar surface chemical status. These results clearly indicate that the CoCN cores play an important role in ORR. The same conclusion can be drawn by comparing the Tafel plots of CoCN@CoO_x(18)/NG,

h-Co_3O_4/NG and Pt/C. As shown in Fig. 4d, the slope of CoCN@CoO_x(18)/NG is -50 mV/decade in 0.1 M KOH, which is obviously lower than those of h-Co_3O_4/NG (-68 mV/decade) and Pt/C (-65 mV/decade), manifesting the higher activity of CoCN@CoO_x core@shell particles than the counterpart hollow oxide spheres.

More experiments were designed to prove the central role of CoCN@CoO_x core@shell particles in ORR. Three CoCN@CoO_x/NG catalysts with different particles sizes were synthesized to investigate the effect of particle size (see ESI and our previous publication[33] for the experimental details). By selecting the deposition method of Co precursor, the average diameter of core@shell particles can be controlled well, as shown in Fig. S5. Three deposition methods, i.e. homogeneous oxidative precipitation (HP), direct impregnation of acetate cobalt (I) and $NH_3 \cdot H_2O$-catalyzed hydrolysis (N) led to particles sizes of 9.2, 12.7 and 14.6 nm, with Co content of 5.0, 7.9 and 4.8 wt%, respectively. However, statistics for TEM images revealed that the same passivation process created the oxide layer in similar thickness of ~2 nm (see Table S4 and Fig. S6), allowing for investigating the effect of CoCN core size. As shown in Fig. 4e, the activity depends on particle size. The larger the CoCN cores, the higher are the ORR activity. Although more studies are yet to be carried out to elucidate the unique size effect, this result indicates that the ORR activity benefits from the higher percentage of CoCN cores.

Differing from the previous publications,[9, 13, 52] the formation of carbonitride implies that the strong interaction between carbon supports and catalytic domains facilitates the ORR reaction. As shown in Figs. 1 and S2, white tortuous trenches

resulted from graphene etching by CoN and the interstitial pores of graphenes endow the catalysts mesoporous feature, which may prevent the restacking and agglomeration of graphene sheets, and improve the accessibility of catalytic domains to oxygen, thereby enhance the activity. Hence, compared to NG from direct nitridation, the activity of washed-NG was higher due to the mesopores left after washed off CoCN@CoO_x NPs, meanwhile the surface chemistry of NG was not changed (See Figs. S7 and S8a for LSV curve and XPS spectrum of washed-NG). Furthermore, we compared the ORR performances of CoN mechanically mixed with washed-NG and CoCN/NG from nitridation and passivation of the mixture of CoO and GO. In the latter, strong interaction between Co domains and NG during the nitridation and passivation may lead to a synergistic effect. This interaction can be identified by their XRD patterns (see Fig. S9 in EIS). The 0.16 ^{o} shift of the (111) reflection of CoCN/NG from CoN+washed-NG suggests the lattice contraction because of the formation of carbide in the CoN NPs. As shown in Fig. S8b, the current density and onset potential of CoCN/NG are superior to those of CoN+washed-NG, suggesting that the interaction between graphene support and Co moieties enhanced their synergy, probably through the formation of cobalt carbide moieties.

As a heterogeneous catalytic process, the elementary steps of cathodic ORR take place on catalyst surfaces.[53] In this work, the essential component CoCN was covered by a layer of oxide. Although it cannot be excluded that there are some micropores through which oxygen directly accesses to CoCN, it is unlikely to dominate the

catalysis, because of the considerable mass-transportation resistance in ORR.[54] For the CoCN@CoO_x catalysts, the oxide layer acts as a protective barrier in the electrolyte, against the fast performance degradation due to CoCN oxidation in the electrolyte. Besides, the catalytic properties of the shell layers might be modified by the CoCN cores with unique electronic structure. Because of the higher electron density near Fermi level caused by d-band contraction, TMNs and TMCs possess good conductivity and the donation of electrons, which favors the activation of oxygen.[55] It might result in an electronic penetration modifying the electron density of oxide layer thin to 2 nm. The scenario is partly supported by the decreased charge transfer resistance of CoCN@CoO_x(18)/NG compared to h-Co_3O_4/NG revealed by the Nyquist plots, as shown in Fig. S10.

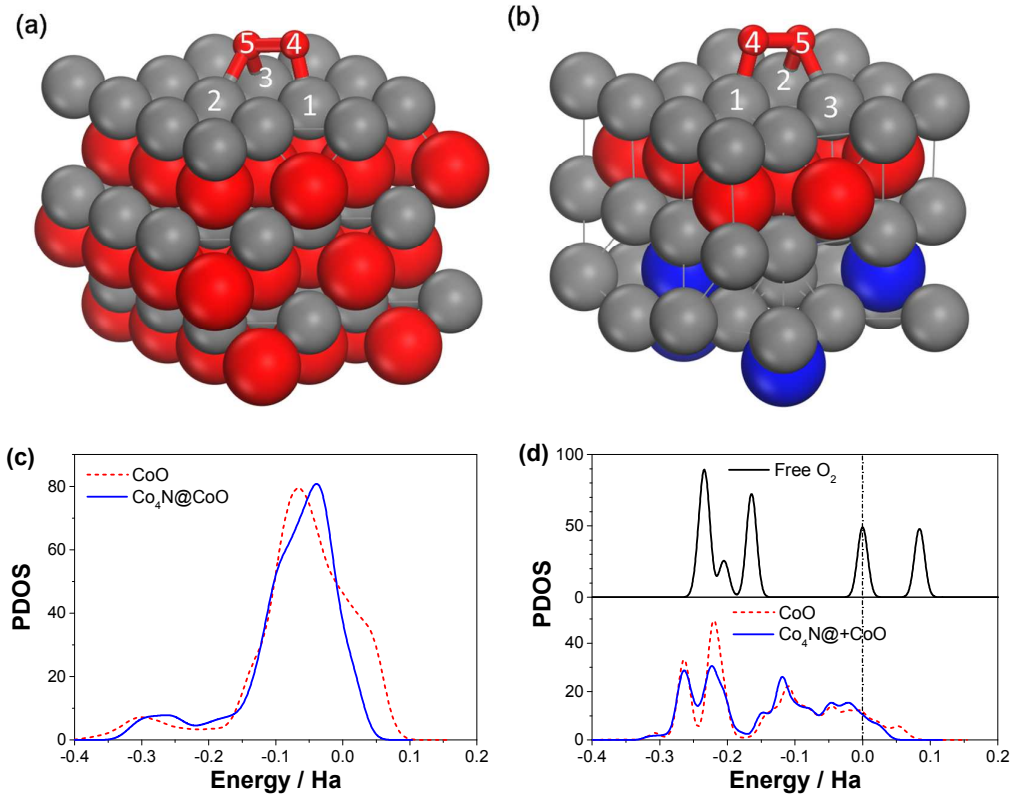

Fig. 5 Stable structures of oxygen adsorption on (a) CoO and (b) Co_4N@CoO. (c) PDOS of cobalt on the surface. Zero energy represents the Fermi level (the same below). (d) PDOS of isolated free oxygen and oxygen 4 in (a) and (b). Unit of PDOS: electrons/Ha.

A DFT calculation was conducted to investigate the electronic structure of CoO modified by Co_4N core. The optimized Co_4N@CoO and CoO structures are shown in Fig. S11 and Table S5. The calculation shows that charges of surface cobalt atoms of CoO increase from 0.088e to 0.108e and 0.118e in the presence of Co_4N, demonstrating the modification of nitride on the electronic structure of CoO shell. The partial density of states (PDOS) analysis of cobalt also shows that the peak of Co_4N@CoO is closer to Fermi level compared with CoO, which indicates that the cobalt on Co_4N@CoO surfaces is more active for electron transfer (Fig. 5c). When an oxygen molecule approaches the surfaces, a stable bridge configuration will be formed via chemisorption with cobalt, as shown in Figs. 5a and b. In detail, one oxygen atom (labeled as 4) is single-bonded to cobalt and the other (labeled as 5) is double-bonded to adjacent two cobalt atoms. As shown in Table S5, electron donation from cobalt to oxygen is revealed by the population analyses of Mulliken charge. The O-O bond in Fig. 5b is longer than that in Fig. 5a (see Table S5), suggesting the readily activation of O_2 over Co_4N@CoO. A PDOS analysis shows that, in the region near the Fermi level (-0.2～0), DOS of O 4 is always greater than O 5 for both of Co_4N@CoO and CoO (Fig. S12), suggesting that the O 4 donates more electrons for the activated orbits. Fig. 5d compares the PDOS of adsorbed O 4 with an isolated oxygen molecule. When an oxygen molecule is adsorbed, electrons will fill in the empty energy level to form new occupied states. The electrons of the newly formed

occupied states are delocalized for electron transfer in ORR. It should be noted that the PDOS of O 4 on Co_4N@CoO is greater than that on CoO near the Fermi level, evidencing that the CoN core increases the density of activated electrons.

Above results display the unique catalysis mode of nanocatalysts with core@shell structure. Similar observations have been reported by several groups across a wide spectrum of heterogeneous catalysis. For instances, a monolayer of Au or Pd atoms may exert extraordinary activity in formic acid and methanol electro-oxidation when coated on Pt;[56, 57] Fe nanowires encapsulated in the channels of CNTs enhanced the catalytic oxidation over CNTs.[58] Fe NPs inside CNTs improved the ORR activity of outer CNTs.[59] In this work, although the direct contacting of absorbents with CoCN surfaces is prohibited, CoCN cores can play the role by affecting the electronic structure of oxide shell from within, providing a new paradigm for core@shell type catalytic nanostructures. This finding is also helpful for understanding the real structure of active sites in Co-N-C systems for ORR.

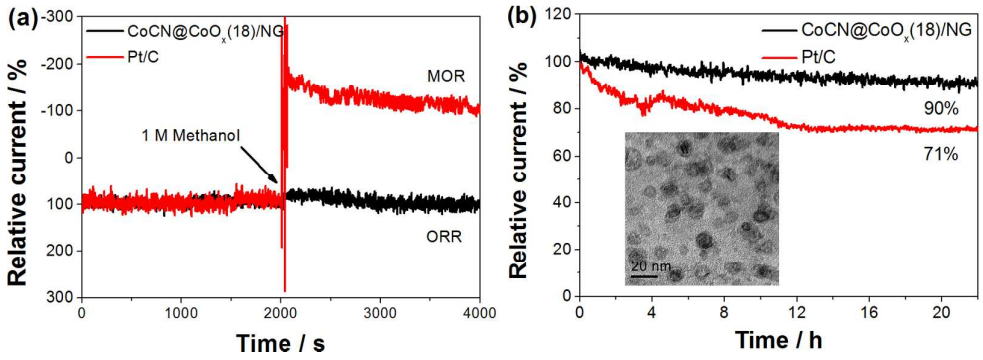

Fig. 6 (a) Current–time (i–t) chronoamperometric responses of CoCN@CoO_x(18)/NG and Pt/C obtained at -0.25 V in O_2-saturated 0.1 M KOH before and after adding 1 M methanol; (b) i-t plots of CoCN@CoO_x(18)/NG and Pt/C at -0.25 V.

To investigate the methanol crossover effect of the catalysts, the electro-oxidation

of methanol in O_2-saturated 0.1 M KOH with 1 M methanol was detected (Fig. 6a). No noticeable change has been observed for CoCN@CoO_x(18)/NG after the addition of methanol in the solution, which means the catalyst possesses a good catalytic selectivity against methanol oxidation in ORR. In the case of commercial Pt/C catalyst, it exhibited a distinct methanol oxidation after methanol introduced into the electrolyte. Furthermore, the durability of CoCN@CoO_x(18)/NG was evaluated by chronoamperometry. As shown in Fig. 6b, CoCN@CoO_x(18)/NG remained 90% of its initial current density after 22 h. It is superior to Pt/C, which lost about 30% activity after the same duration in alkaline solution. Morphology of the catalyst after stability test was observed by TEM. As shown in inset of Fig. 5b, most of the particles remained the core@shell structure. A statistic indicated that the percentage of hollow NPs increased from 6.5% to 10%, caused by the gradual oxidation of CoCN into CoO_x during the reaction. Although it was probably responsible for the slight performance fading, the remarkable enhancement of stability compared to Pt/C demonstrated that CoCN@CoO_x(18)/NG is a promising catalyst for ORR in alkaline medium.

Conclusions

In summary, a new hybrid catalyst in the form of CoCN@CoO_x NPs supported on N-doped graphenes has been designed for ORR in alkaline solution. The catalyst particles show a core@shell structure, in which the oxide acts as a protective layer, thin to 2 nm, to prevent the oxidation corrosion of CoCN. And the CoCN core plays a decisive role in ORR by modifying the electronic structure of CoO_x shell to improve

the activation of oxygen, which is shown by LSV measurements and DFT calculations. CoCN@CoO_x(18)/NG displays a competitive ORR activity to commercial Pt/C catalysts, featured by high activity, good selectivity and durability. The high performance benefits from the synergistic effect between the CoCN@CoO_x NPs and the mesoporous N-doped graphenes, highlighting a promising alternative to noble metal catalysts owing to its Pt-like performance and low cost.

Acknowledgements

This work is supported by the National Science Foundation of China (No. 21273079), the Guangdong Provincial National Science Foundation of China (Nos. 9251064101000020, S20120011275), Program for New Century Excellent Talents in University (NCET-12-0190), and the Fundamental Research Funds for the Central Universities of China (No. 2014ZG0005). We are thankful to the help of Dr. Zheng Liu at Rice University that he provided in the HREM and EELS characterizations of our samples.

Notes and references

*School of Chemistry and Chemical Engineering, South China University of Technology, Guangzhou, 510640, China.

Email: yuhao@scut.edu.cn (H.Y.); cefpeng@scut.edu.cn (F.P.); Tel. & Fax.: +86-20-8711 4916

†Electronic supplementary information (ESI) available: calculation methods for K-L plots and Tafel plots, synthesis and characterization of CoCN@CoO_x/NG with

different particles sizes, and supplementary results with figures and tables are included.

1. H. A. Gasteiger, S. S. Kocha, B. Sompalli and F. T. Wagner, *Appl. Catal. B-Environ.*, 2005, **56**, 9-35.
2. I. E. L. Stephens, A. S. Bondarenko, U. Gronbjerg, J. Rossmeisl and I. Chorkendorff, *Energy Environ. Sci.*, 2012, **5**, 6744-6762.
3. Y. Liu, A. Ishihara, S. Mitsushima, N. Kamiya and K. Ota, *J. Electrochem. Soc.*, 2007, **154**, B664-B669.
4. R. W. Reeve, P. A. Christensen, A. Hamnett, S. A. Haydock and S. C. Roy, *J. Electrochem. Soc.*, 1998, **145**, 3463-3471.
5. K. Lee, A. Ishihara, S. Mitsushima, N. Kamiya and K.-I. Ota, *Electrochim. Acta*, 2004, **49**, 3479-3485.
6. G.-Q. Sun, J.-T. Wang, S. Gupta and R. F. Savinell, *J. Appl. Electrochem.*, 2001, **31**, 1025-1031.
7. R. B. Levy and M. Boudart, *Science*, 1973, **181**, 547-549.
8. E. Furimsky, *Appl. Catal. A-Gen.*, 2003, **240**, 1-28.
9. J. Chen, K. Takanabe, R. Ohnishi, D. L. Lu, S. Okada, H. Hatasawa, H. Morioka, M. Antonietti, J. Kubota and K. Domen, *Chem. Commun.*, 2010, **46**, 7492-7494.
10. L. Liao, X. J. Bian, J. J. Xiao, B. H. Liu, M. D. Scanlon and H. H. Girault, *Phys. Chem. Chem. Phys.*, 2014, **16**, 10088-10094.
11. H. X. Zhong, H. M. Zhang, G. Liu, Y. M. Liang, J. W. Hu and B. L. Yi, *Electrochem. Commun.*, 2006, **8**, 707-712.
12. M. Chisaka, T. Iijima, T. Yaguchi and Y. Sakurai, *Electrochim. Acta*, 2011, **56**, 4581-4588.
13. A. Ishihara, M. Tamura, Y. Ohgi, M. Matsumoto, K. Matsuzawa, S. Mitsushima, H. Imai and K.-I. Ota, *J. Phys. Chem. C*, 2013, **117**, 18837-18844.
14. I. Milad, K. Smith, P. Wong and K. Mitchell, *Catal. Lett.*, 1998, **52**, 113-119.
15. S. Chouzier, M. Vrinat, T. Cseri, M. Roy-Auberger and P. Afanasiev, *Appl. Catal. A-Gen.*, 2011, **400**, 82-90.
16. D. Ham and J. Lee, *Energies*, 2009, **2**, 873-899.
17. T. Ando, S. Izhar, H. Tominaga and M. Nagai, *Electrochim. Acta*, 2010, **55**, 2614-2621.
18. M. Chisaka, A. Ishihara, K.-I. Ota and H. Muramoto, *Electrochim. Acta*, 2013, **113**, 735-740.
19. Z. W. Yao, X. H. Zhang, F. Peng, H. Yu, H. J. Wang and J. A. Yang, *Int. J. Hydrogen Energy*, 2011, **36**, 1955-1959.
20. B. F. Cao, G. M. Veith, R. E. Diaz, J. Liu, E. A. Stach, R. R. Adzic and P. G.

Khalifah, *Angew. Chem. Int. Ed.*, 2013, **125**, 10953-10957.
21. K. P. Gong, F. Du, Z. H. Xia, M. Durstock and L. M. Dai, *Science*, 2009, **323**, 760-764.
22. L. T. Qu, Y. Liu, J. B. Baek and L. M. Dai, *Acs Nano*, 2010, **4**, 1321-1326.
23. Y. Zheng, Y. Jiao, L. Ge, M. Jaroniec and S. Z. Qiao, *Angew. Chem. Int. Ed.*, 2013, **125**, 3192-3198.
24. L. M. Dai, *Acc. Chem. Res.*, 2012, **46**, 31-42.
25. X.-K. Kong, C.-L. Chen and Q.-W. Chen, *Chem. Soc. Rev.* , 2014, **43**, 2841-2857.
26. Y. Y. Liang, Y. G. Li, H. L. Wang, J. G. Zhou, J. Wang, T. Regier and H. J. Dai, *Nat. Mater.*, 2011, **10**, 780-786.
27. Y. G. Li, W. Zhou, H. L. Wang, L. M. Xie, Y. Y. Liang, F. Wei, J.-C. Idrobo, S. J. Pennycook and H. J. Dai, *Nat. Nanotechnol.*, 2012, **7**, 394-400.
28. H. B. Yin, C. Z. Zhang, F. Liu and Y. L. Hou, *Adv. Funct. Mater.*, 2014, **24**, 2930-2937.
29. N. I. Kovtyukhova, P. J. Ollivier, B. R. Martin, T. E. Mallouk, S. A. Chizhik, E. V. Buzaneva and A. D. Gorchinskiy, *Chem. Mater.*, 1999, **11**, 771-778.
30. Y.-S. Jun, W. H. Hong, M. Antonietti and A. Thomas, *Adv. Mater.*, 2009, **21**, 4270-4274.
31. B. Delley, *J. Chem. Phys.* , 2000, **113**, 7756-7764.
32. J. P. Perdew, K. Burke and M. Ernzerhof, *Phys. Rev. Lett.* , 1997, **78**, 1396-1396.
33. Y. S. Wu, H. Yu, H. J. Wang and F. Peng, *Chin. J. Catal.*, 2014, **35**, 952-959.
34. F. Jaouen, J. Herranz, M. Lefevre, J. P. Dodelet, U. I. Kramm, I. Herrmann, P. Bogdanoff, J. Maruyama, T. Nagaoka, A. Garsuch, J. R. Dahn, T. Olson, S. Pylypenko, P. Atanassov and E. A. Ustinov, *ACS Appl. Mater. Interfaces*, 2009, **1**, 1623-1639.
35. S. Li, L. Zhang, H. S. Liu, M. Pan, L. Zan and J. J. Zhang, *Electrochim. Acta*, 2010, **55**, 4403-4411.
36. N. Severin, S. Kirstein, I. M. Sokolov and J. P. Rabe, *Nano Lett.*, 2009, **9**, 457-461.
37. C. M. Schumacher, F. M. Koehler, A. C. C. Rotzetter, R. A. Raso and W. J. Stark, *J. Phys. Chem. C*, 2012, **116**, 13693-13698.
38. W. S. Wang, M. Dahl and Y. D. Yin, *Chem. Mater.*, 2012, **25**, 1179-1189.
39. H. F. Xiong, M. Moyo, M. A. M. Motchelaho, L. L. Jewell and N. J. Coville, *Appl. Catal. A-Gen.*, 2010, **388**, 168-178.
40. A. L. da Silva, J. P. den Breejen, L. V. Mattos, J. H. Bitter, K. P. de Jong and F. B. Noronha, *J. Catal.* , 2014, **318**, 67-74.
41. G. L. Bezemer, J. H. Bitter, H. Kuipers, H. Oosterbeek, J. E. Holewijn, X. D. Xu, F. Kapteijn, A. J. van Dillen and K. P. de Jong, *J. Am. Chem. Soc.*, 2006, **128**, 3956-3964.
42. Z. Li, J. Liu, Z. Huang, Y. Yang, C. Xia and F. Li, *ACS Catal.*, 2013, **3**, 839-845.
43. V. G. Hadjiev, M. N. Iliev and I. V. Vergilov, *J. Phys. C-Solid State Phys.*,

1988, **21**, L199.
44. C.-W. Tang, C.-B. Wang and S.-H. Chien, *Thermochim. Acta*, 2008, **473**, 68-73.
45. D. Gallant, M. Pézolet and S. Simard, *J. Phys. Chem. B*, 2006, **110**, 6871-6880.
46. D. T. Dam, K.-D. Nam, H. Song, X. Wang and J.-M. Lee, *Int. J. Hydrogen Energy*, 2012, **37**, 15135-15139.
47. B. F. Cao, G. M. Veith, J. C. Neuefeind, R. R. Adzic and P. G. Khalifah, *J. Am. Chem. Soc.*, 2013, **135**, 19186-19192.
48. T. J. Chuang, C. R. Brundle and D. W. Rice, *Surf. Sci.*, 1976, **59**, 413-429.
49. J. Xu, P. Gao and T. Zhao, *Energy Environ. Sci.*, 2012, **5**, 5333-5339.
50. Z. H. Xiang, Y. H. Xue, D. P. Cao, L. Huang, J. F. Chen and L. M. Dai, *Angew. Chem. Int. Ed.*, 2014, **53**, 2433-2437.
51. S. J. Guo, S. Zhang, L. Wu and S. H. Sun, *Angew. Chem. Int. Ed.*, 2012, **124**, 11940-11943.
52. C. W. Tsai, H. M. Chen, R. S. Liu, K. Asakura, L. Zhang, J. J. Zhang, M. Y. Lo and Y. M. Peng, *Electrochim. Acta*, 2011, **56**, 8734-8738.
53. J. B. Wu and H. Yang, *Acc. Chem. Res.*, 2013, **46**, 1848-1857.
54. H. Rismani-Yazdi, S. M. Carver, A. D. Christy and I. H. Tuovinen, *J. Power Sources*, 2008, **180**, 683-694.
55. S. T. Oyama, *Catal. Today*, 1992, **15**, 179-200.
56. X. X. Bi, R. Y. Wang and Y. Ding, *Electrochim. Acta*, 2011, **56**, 10039-10043.
57. Y. L. Du, K. L. Lv, B. Q. Su, N. O. Zhang and C. M. Wang, *J. Appl. Electrochem.*, 2009, **39**, 2409-2414.
58. X. X. Yang, H. Yu, F. Peng and H. J. Wang, *ChemSusChem*, 2012, **5**, 1213-1217.
59. D. H. Deng, L. Yu, X. Q. Chen, G. X. Wang, L. Jin, X. L. Pan, J. Deng, G. Q. Sun and X. H. Bao, *Angew. Chem. Int. Ed.*, 2013, **52**, 371-375.

Graphical Abstract

Nitrogen-doped Graphene-Supported Cobalt Carbonitride@Oxide Core-Shell Nanoparticles as a Non-noble Metal Electrocatalyst for Oxygen Reduction Reaction

Yingsi Wu, Qianqian Shi, Yuhang Li, Zhuangchai Lai, Hao Yu*, Hongjuan Wang, Feng Peng*

School of Chemistry and Chemical Engineering, South China University of Technology, Guangzhou, 510640, China. Email: yuhao@scut.edu.cn (H.Y.); cefpeng@scut.edu.cn (F.P.); Tel. & Fax.: +86-20-8711 4916.

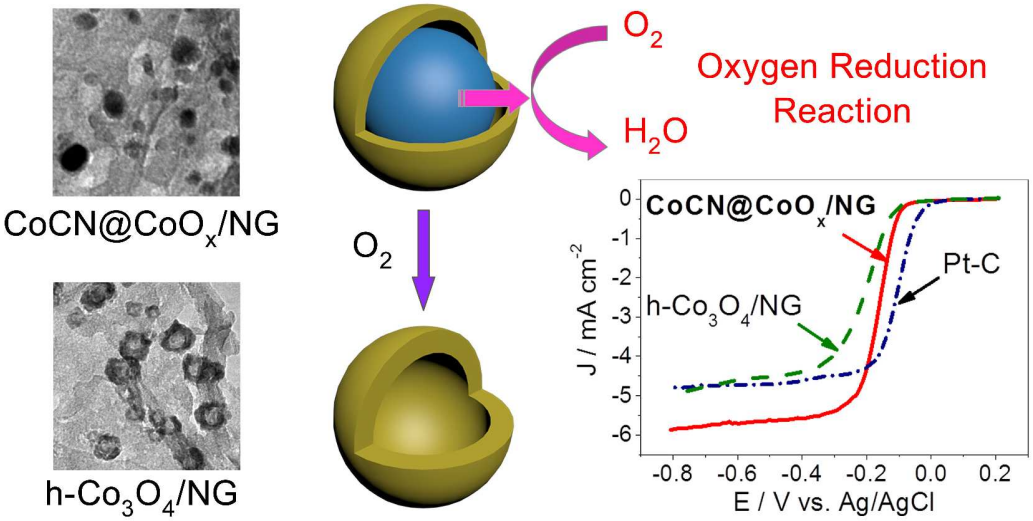

Cobalt carbonitride (CoCN) nanoparticles supported on nitrogen-doped graphene (NG), showing a core-shell structure with a highly active CoCN core and a protective cobalt oxide shell, present excellent activity in ORR compared to cobalt oxide supported on NG and commercial Pt/C catalysts, benefiting from the strong

synergistic effect between CoCN and NG and the electronic modification of cobalt oxide by CoCN from within.